https://doi.org/10.5194/egusphere-2026-4226
Preprint. Discussion started: 28 July 2026

Uncertainty in root zone storage capacity estimates and its implications for hydrological modelling

Muhammad Ibrahim[1], Markus Hrachowitz[1], Miriam Coenders-Gerrits[1], Ruud van der Ent[1]

[1]Department of Water Management, Faculty of Civil Engineering and Geosciences, Delft University of Technology, Delft, The Netherlands

Correspondence to: Muhammad Ibrahim (m.ibrahim@tudelft.nl)

Abstract. In hydrological and land-surface models, root zone storage ($S_{r,max}$) plays a fundamental role in the partitioning of terrestrial water fluxes and, consequently, in the ability of vegetation to withstand dry periods. It represents the maximum volume of subsurface water that can be accessed by vegetation to sustain transpiration. As direct measurements of rooting depth are generally unavailable at the catchment scale, $S_{r,max}$ is inferred either through hydrological model calibration or by applying the memory method. The memory method estimates $S_{r,max}$ from a series of annual maximum water storage deficits based on an assumed extreme value distribution, commonly the Gumbel distribution, and a fixed 20-year return period. However, the uncertainties in $S_{r,max}$ estimates associated with these assumptions have not been systematically quantified. Here, we systematically quantify and evaluate these uncertainties across ~5700 catchments worldwide by replacing Gumbel distribution with the more flexible Generalized Extreme Value (GEV) distribution and applying a bootstrap framework to derive uncertainty bounds on $S_{r,max}$. Analysis of the GEV shape parameter (ξ) shows a strong hydroclimatic control. Most catchments in water-limited environments are characterized by a negative ξ, indicative of bounded extremes: extension of root systems beyond these bounds does not have benefits for vegetation as most of the available water is already used by vegetation. In contrast, positive values of ξ are more commonly found in energy-limited catchments, indicating a heavy tailed distribution of annual maximum water storage deficits. This implies that vegetation benefits from adapting root systems and thus $S_{r,max}$ to dry periods with longer return periods, as in these environments sufficient water is available in the subsurface to be accessed and used by these larger root systems. Overall, uncertainties in $S_{r,max}$ estimates varied systematically across climatic conditions. The widest uncertainty ranges were observed in transitional climates (aridity index 0.5–2) with a median value of approximately ± 66 mm, whereas humid and arid regions exhibited substantially smaller uncertainty ranges (median ~± 36 mm). Using these uncertainty ranges as calibration bounds for $S_{r,max}$ in a hydrological model resulted in many parameter sets yielding comparable model performance for the majority of catchments. Yet memory method $S_{r,max}$ estimates show a strong agreement with median calibrated $S_{r,max}$ values, with a *RMSE* ~50 mm and a global Pearson correlation coefficient of $\rho = 0.93$, with ρ ranging from 0.91 to 0.98 across different climate zones. The strongest agreement between calibrated and memory method estimates of $S_{r,max}$ is consistently found for return periods of 20–30 years, with higher sensitivity in cold and temperate regions. Overall, the findings of this study demonstrate that the memory method is robust in capturing $S_{r,max}$ spatial patterns. They also suggest that the use of a 20-

https://doi.org/10.5194/egusphere-2026-4226
Preprint. Discussion started: 28 July 2026

year return period is supported by underlying hydroclimatic behaviour and physically processes, rather than being an arbitrary assumption. Memory method based estimates of $S_{r,max}$ provide an alternative to calibration, thereby reducing model complexity and parameter uncertainty while preserving model performance, particularly in large scale hydrological and land-surface modelling.

1 Introduction

Hydrological and land-surface models rely on conceptual representation of subsurface storage components to simulate key hydrological components such as evaporation and runoff generation (Clark et al., 2015; Hrachowitz and Clark, 2017). An important component of this subsurface storage is the root zone, which primarily regulates the availability of water to vegetation during dry periods and links soil moisture dynamics not only to energy exchange fluxes between the land-surface and the atmosphere but also to evaporation (Milly, 1994; Porporato et al., 2004; Seneviratne et al., 2010; Fatichi et al., 2015; Wang-Erlandsson et al., 2016; Gao et al., 2024), which constitutes the largest fraction of all of atmospheric fluxes (Jasechko, 2018), while at the same time also presenting the largest source of uncertainty (Coenders-Gerrits et al., 2014). Through this role of sustaining evaporation, the root zone buffers catchment-scale water balance dynamics (Ibrahim et al., 2026). This buffering role of root zone is frequently described through the concept of root zone storage capacity ($S_{r,max}$), which is defined as the maximum subsurface water volume accessible to plants to meet their transpiration needs (Gao et al., 2014), making it a key part of terrestrial hydrological systems as it regulates the partitioning of water into evaporation (Savenije and Hrachowitz, 2017). Consequently, robust estimates of $S_{r,max}$ are essential for robust process representation in and predictive capability of hydrological and land-surface models.

Despite its importance, $S_{r,max}$ cannot be directly observed at catchment scale. Field measurements of rooting depth and soil water storage are representative of only a specific point and integration of this point measurement to catchment scale is challenging due to spatial heterogeneity nature of catchments (De Boer-Euser et al., 2016; Hrachowitz et al., 2021). Consequently, $S_{r,max}$ is commonly considered as a calibration parameter in hydrological models. Though calibration can result in satisfactory model performance, it is often associated with parameter equifinality where multiple parameter sets can produce similar simulations of observed fluxes (Beven and Freer, 2001). This limits processes interpretability and increases uncertainty in model predictions particularly under changing hydroclimatic conditions (Hrachowitz et al., 2014; Beven, 2019; Boardman et al., 2025). To address these limitations, several functionally equivalent approaches to estimate $S_{r,max}$ from readily available water balance data have been proposed and are often referred to as memory method, water balance method or mass curve technique (Gao et al., 2014; Nijzink et al., 2016; Wang-Erlandsson et al., 2016; Bouaziz et al., 2020; Van Oorschot et al., 2021). In this approach, $S_{r,max}$ is derived from annual maximum storage deficits (S_d) that are estimated from long-term water balance data (details can be found in Van Oorschot et al. (2024)). This approach is based on the concept that current $S_{r,max}$ is a

https://doi.org/10.5194/egusphere-2026-4226
Preprint. Discussion started: 28 July 2026

manifestation of past water deficits. In other words, vegetation that is present, has successfully adjusted its root systems to have survived past dry periods. As such, vegetation keeps memory of environmental conditions in such a way that it adapts the extents of its root systems efficiently to fulfil its transpiration needs during dry periods. This approach has been widely adopted for estimation of the extent of vegetation root zones i.e., $S_{r,max}$ (Donohue et al., 2012; Gentine et al., 2012; Wang-Erlandsson et al., 2016; Dralle et al., 2021; Mccormick et al., 2021; Stocker et al., 2023).

The memory method has also been widely applied and tested in modelling studies across diverse hydroclimatic regions (Wang-Erlandsson et al., 2016; Hrachowitz et al., 2021; Van Oorschot et al., 2021; Stocker et al., 2023; Tempel et al., 2024; Wang et al., 2024; Ponds et al., 2025), providing an alternative to the calibration-based $S_{r,max}$ determination. Recent global scale work by Ibrahim et al. (2026) has shown that $S_{r,max}$ is closely linked to long-term precipitation partitioning, reinforcing its relevance for catchment scale water balance dynamics. However, despite its widespread use, several underlying assumptions of the method remain insufficiently tested at large scales. The first assumption is the common use of the Gumbel distribution as a fixed extreme value distribution to estimate $S_{r,max}$ associated with specific dry spell return periods. This assumption entails a specific tail behaviour on annual maximum storage deficits (S_d), which directly influences the extrapolation of storage deficits and therefore the resulting $S_{r,max}$ estimates. However, hydrological extremes are known to exhibit spatially variable tail characteristics (Katz et al., 2002), which may be better captured by the more flexible Generalized Extreme Value (GEV) distribution (Coles et al., 2001). The GEV framework is defined by the shape parameter ξ. Depending on ξ, the GEV is equivalent to the Gumbel ($\xi = 1$), Fréchet ($\xi > 1$), and reversed Weibull type distributions ($\xi < 1$). It therefore allows a flexible representation of both, bounded and heavy tailed distributions of extreme events. Whether the use of a fixed Gumbel distribution is reasonable and robust across a diverge range of hydroclimatic regions remains largely unexplored.

Another frequent key assumption of the memory method is the use of a fixed return period of 20 years for calculation of $S_{r,max}$ that is based on the conceptual understanding of the vegetation adaptation to the drought buffering. This use of a 20-year return period is rarely scrutinized and its hydroclimatic consistency across different hydroclimatic regions remains unclear. Further, as reported by Katz et al. (2002), hydrological extremes are known to vary systematically with climatic conditions, both the appropriate return period and the associated $S_{r,max}$ are also expected to exhibit climate dependence. Furthermore, many implementations of the memory method estimate a single deterministic value of $S_{r,max}$ for a 20-year return period without explicitly considering the uncertainty associated with extreme value estimation. This may lead to a deceptive sense of accuracy as in reality, uncertainties in estimates of $S_{r,max}$ due to choices of extreme value distributions and dry spell return periods need to be expected. Neglecting these uncertainties may limit the robustness of the model parameterization and its propagation into hydrological simulations. This highlights the need to explicitly quantify the uncertainty in $S_{r,max}$ associated with different extreme value distributions and return periods and analyse its implications in hydrological modelling.

https://doi.org/10.5194/egusphere-2026-4226
Preprint. Discussion started: 28 July 2026

This study investigates the uncertainty, robustness, and practical implications of memory method based estimates of $S_{r,max}$ across approximately 5700 catchments spanning a wide range of hydroclimatic conditions. Specifically, we replaced the commonly used Gumbel distribution with the more flexible GEV distribution to allow for a better representation of tail behaviour of annual maximum storage deficits. We further analyse spatial patterns of the GEV shape parameter and examine its hydroclimatic controls. Building on this, we quantify the uncertainty in $S_{r,max}$ estimates using a bootstrap resampling approach and express it in terms of a range of plausible values associated with different return periods (5-year and 80-year). Finally, to evaluate the practical relevance of these uncertainties, we use the derived $S_{r,max}$ bounds in a hydrological model and compare it to calibrated values across approximately 2100 catchments and analyse the impact on model performance and parameter estimation. This study provides the first systematic large-scale analysis of the robustness and practical applicability of memory method $S_{r,max}$ estimates across diverse hydroclimatic regions by evaluating distributional assumptions, quantifying associated uncertainties across return periods, and examining their practical utility for large-scale hydrological modelling.

2 Datasets and methods

2.1 Meteorological and hydrological data

This study uses hydrological and meteorological datasets comprising 5717 catchments worldwide covering a wide range of hydroclimatic conditions (Ibrahim et al., 2026). The datasets include daily precipitation P [mm d^{-1}], daily minimum and maximum temperature T [°C], daily potential evaporation E_P [mm d^{-1}] estimated using the Hargreaves and Samani (1982) method, and streamflow Q data obtained from the sources as mentioned in Table 1. The analysis period spans from 1981 to 2010. Catchment selection criteria and preprocessing procedures follow Ibrahim et al. (2026) (see Table 1) to ensure consistency with previous work. The selected catchments mainly satisfy three criteria: (1) a minimum of 20 years of streamflow data within the study period, (2) a maximum catchment area of 10,000 km² to limit spatial heterogeneity, and (3) a non-negative long-term water balance (i.e., $\bar{P} - \bar{Q} \geq 0$) to avoid inconsistencies in the underlying data.

https://doi.org/10.5194/egusphere-2026-4226
Preprint. Discussion started: 28 July 2026

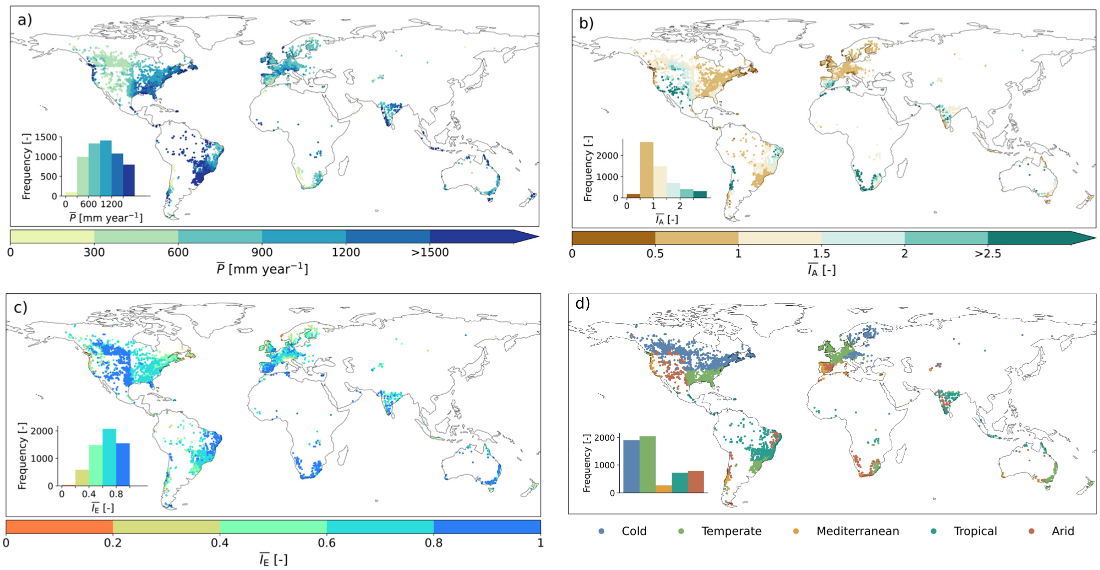

Figure 1: Global distribution of the study catchments (n = 5717) together with their long term mean (1981–2010) hydroclimatic characteristics: (a) mean annual precipitation $\overline{P}$, (b) aridity index $\overline{I_A} = \overline{E_P}/\overline{P}$, where $\overline{E_P}$ is long-term mean potential evaporation calculated using the Hargreaves and Samani (1982) method, (c) evaporative index $\overline{I_E} = \overline{E_A}/\overline{P}$, where $\overline{E_A}$ is actual evaporation derived from the long term water balance ($\overline{P} - \overline{Q} - \mathrm{d}S/\mathrm{d}t$) assuming negligible long term storage change (30-years) (Han et al. (2020)), and (d) Köppen-Geiger climate classes: cold (Dfa, Dfb, Dfc), temperate (Cwa, Cwb, Cfa, Cfb), Mediterranean (Csa, Csb), tropical (Af, Am, Aw), and arid (BWh, BWk, BSh, BSk). The above hydroclimatological input datasets and catchment selection are identical to those used in Ibrahim et al. (2026).

https://doi.org/10.5194/egusphere-2026-4226
Preprint. Discussion started: 28 July 2026

Table 1: Hydro-meteorological variables used in the estimation of $S_{r,max}$ and hydrological modelling, including corresponding symbols, units and data sources

Variable	Symbol	Units	Data source
Hydro-meteorological variables			
Precipitation	P	mm d^{-1}	Global Soil Wetness Project Phase-3 (GSWP-3) (Dirmeyer et al., 2006)
Temperature	T	°C	Global Soil Wetness Project Phase-3 (GSWP-3) (Dirmeyer et al., 2006)
Potential evaporation	E_P	mm d^{-1}	Hargreaves and Samani (1982)
Long-term streamflow (for calculation of $S_{r,max}$) 5717 catchments	$\bar{Q}$	mm d^{-1}	Global Streamflow Indices and Metadata (GSIM) archive (Do et al., 2018; Gudmundsson et al., 2018) Caravan (Kratzert et al., 2023) African Database of Hydrometric Indices (ADHI) (Tramblay et al., 2021) Central Asia -Discharge (Marti et al., 2023)
Daily Streamflow (for hydrological modelling and calibration) 2111 catchments	Q	mm d^{-1}	ESTREAMS (Do Nascimento et al., 2024) CAMELS-USA (Newman et al., 2015) CAMELS-GB (Coxon et al., 2020) CAMELS-BR (Chagas et al., 2020) CAMELS-CL(Alvarez-Garreton et al., 2018) CAMELS-AUS (Fowler et al., 2021) CAMELS-NZ (Bushra et al., 2025) CAMELS-DE (Loritz et al., 2024) CAMELS-IND (Mangukiya et al., 2025) CAMELS-FR (Delaigue et al., 2025) HYSETS (Arsenault et al., 2020) GRDC
Seasonality index of liquid precipitation input	I_S	[-]	(Gao et al., 2014)

2.2 Methods

Calculation of $S_{r,max}$ and uncertainty quantification

We calculated root zone storage $S_{r,max}$ for each catchment by using the memory method (Van Oorschot et al., 2021). In this method, a long-term daily storage deficit (S_d) time series is derived from the catchment scale water balance data following the methodology described by Van Oorschot et al. (2024) and a conceptual diagram is depicted by Ibrahim et al. (2026). From this daily time series of S_d, annual maximum storage deficits are extracted to quantify the amount of water

https://doi.org/10.5194/egusphere-2026-4226
Preprint. Discussion started: 28 July 2026

available to roots of vegetation for transpiration needs during dry periods (Bouaziz et al., 2022). In the traditional memory method, a Gumbel distribution is fitted to the annual maximum S_d series and $S_{r,max}$ is defined as the storage deficit corresponding to a fixed return period, typically of 20 years as shown in Fig. 2b.

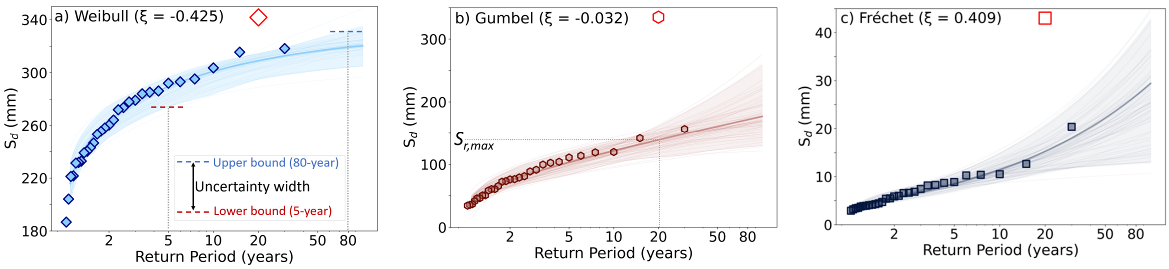

Figure 2: A conceptual illustration of three types of GEV distribution tail behaviour and their link to memory method based $S_{r,max}$ estimation, using three characteristic example catchments. Tail behaviour of the GEV distribution depends on its shape parameter (ξ) value. Negative ξ values correspond to bounded (Weibull-type) extremes (panel a), ξ ≈ 0 represents Gumbel-type behaviour (panel b), and positive ξ values indicate heavy-tailed (Fréchet-type) behaviour (panel c). In the memory method, $S_{r,max}$ is defined as the storage deficit (S_d) corresponding to a 20-year return period under a fixed Gumbel assumption as shown by the dotted intersection lines in panel b. A schematic illustration of the calculation of uncertainty in memory method derived $S_{r,max}$ estimates based on GEV fitting and return period selection is shown in panel a. Uncertainty associated with the GEV fit is quantified by using bootstrap resampling. Light colour curves represent GEV fits obtained from individual bootstrap samples. The shaded region shows the 5th–95th percentile confidence envelope derived from the bootstrap ensemble across return periods. Uncertainty width is calculated as the difference between the upper and lower confidence bounds for return periods between 5 and 80 years. The red markers at the top of each panel refers to the characteristic example catchments shown in Figs. 3 and 5. The other markers on the curves are the maximum observed annual storage deficits (S_d).

However, in this study, we systematically extended the memory method by replacing the fixed Gumbel distribution with a more flexible Generalized Extreme Value (GEV) distribution that allows a better data driven representation of tail behaviour of maximum annual storage deficits. The GEV distribution consists of three parameters referred to as location (μ), scale (σ) and shape (ξ) parameters. The shape parameter controls the tail behaviour of GEV distribution and enables distinction between the three types of GEV distributions: Weibull (ξ < 0; Fig. 2a), which have bounded extremes, Gumbel (ξ = 0; Fig. 2b), and Fréchet (ξ > 0; Fig. 2c), which exhibits heavy-tailed behaviour.

Furthermore, to quantify the uncertainty associated with $S_{r,max}$ estimates, we applied a bootstrap resampling approach (200 samples) to the annual maximum S_d series and derived confidence bounds based on a range of return periods (5-years to 80-years). These bounds represent the plausible range of $S_{r,max}$ values and are subsequently used to assess the sensitivity of $S_{r,max}$ to the return period selection and to propagate uncertainty into hydrological model calibration. An illustrative example of calculation of this uncertainty quantification is shown in Fig. 2a.

https://doi.org/10.5194/egusphere-2026-4226
Preprint. Discussion started: 28 July 2026

Hydrological modelling and calibration:

To analyse the practical implications of the uncertainty in $S_{r,max}$, we employed a simple process-based lumped hydrological model built upon the DYNAMIT modelling framework (Hrachowitz et al., 2014; Wang et al., 2024). This model was selected to ensure computational efficiency during calibration, keeping in view the large spatial scale of the study (~2100 catchments). Moreover, considering the inherent complexity of dominant hydrological process (Ye et al., 2012) and the limited availability of detailed observation data, this modelling approach represents a reasonable choice. A schematic of the model structure along with related processes equations are provided in Supplement S1.

Model calibration was performed for each catchment using daily observed streamflow data obtained from the sources listed in Table 1. Only catchments with at least 10 years of streamflow observations data within the study period (1981–2010) were retained for hydrological modelling, resulting in a total of 2111 catchments. We used a Monte Carlo sampling approach for calibration of 10 model parameters with at least 10000 simulations per catchment on a daily time step keeping in view the large sample and computational resources required. Model parameters were sampled from predefined uniform prior distributions based on previous studies (Table S2). However, for $S_{r,max}$ as parameter, we constrained its range with values derived from the memory method based bootstrap analysis as discussed in the previous section (Fig. 2a). Specifically, $S_{r,max}$ was sampled from uncertainty bounds associated with return periods from 5 years to 80 years, thereby explicitly incorporating observational and statistical uncertainty into the calibration process.

Model calibration was evaluated using Nash–Sutcliffe efficiencies of streamflow (NSE_Q), the logarithm of streamflow ($NSE_{log(Q)}$) and monthly runoff coefficients (NSE_{RC}) to better represent the high flows, low flows and long-term water balance behaviour of hydrograph respectively (e.g., Bouaziz et al. (2022)). Among all parameter sets, we only retained those which exceed a threshold value of 0.1 for all three objective functions. Rather than selecting a single optimal solution, we rank all the retained parameter sets according to the Euclidian distance (D_E) to the perfect model (e.g., Hulsman et al. (2020)) and then selected the top 150 Pareto-optimal solutions for each catchment to construct uncertainty intervals. Comparing the $S_{r,max}$ distributions of the retained calibrated solutions to the $S_{r,max}$ estimates obtained from the memory method then allowed us to evaluate the extent to which $S_{r,max}$ obtained from the memory method can replace calibration while maintaining model performance and to assess the impact of its uncertainty on parameter equifinality and model robustness.

3 Results

To describe how different shapes of GEV distributions (instead of a fixed Gumbel distribution) propagate uncertainties into of $S_{r,max}$ estimates, we first examine how the GEV shape parameter (ξ) varies across different hydroclimatic

https://doi.org/10.5194/egusphere-2026-4226
Preprint. Discussion started: 28 July 2026

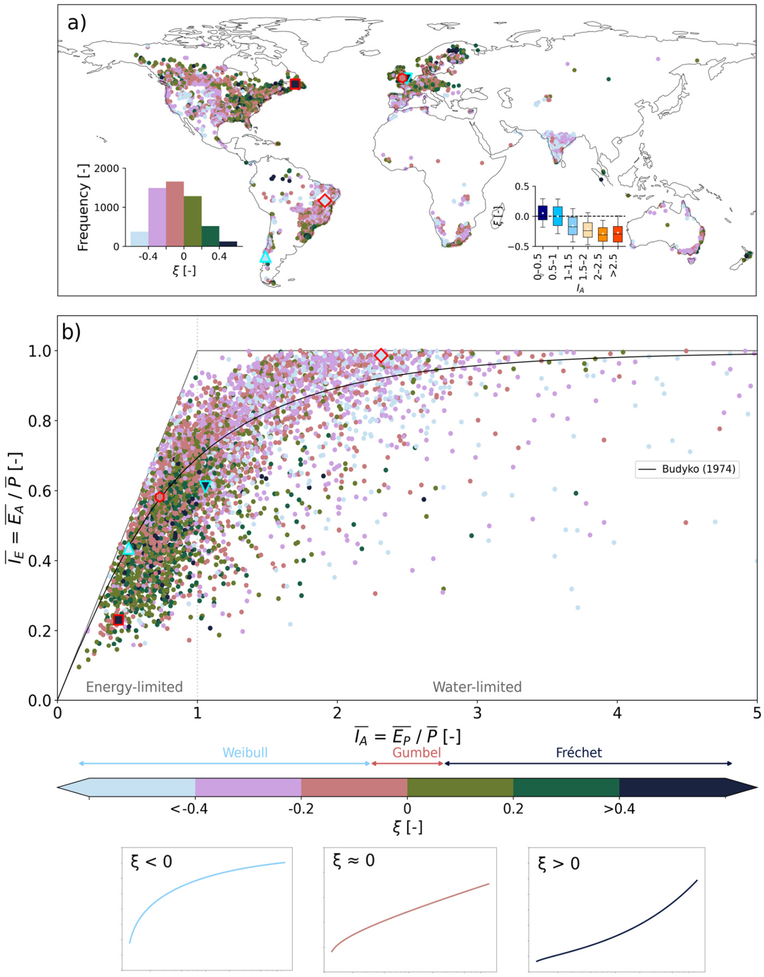

Figure 3: (a) Global distribution of the GEV distribution shape parameter (ξ). The inset boxplots show the variation of ξ across different aridity index classes. The boxplots illustrate 25th –75th percentile range, whiskers extend to the 10th and 90th percentiles, white diamonds denote the arithmetic means, and outliers are excluded for better visualization. (b) ξ variation in the Budyko framework. The catchments highlighted with red border in panels a and b correspond to the three characteristic example catchments illustrating different GEV tail behaviours, as shown in Fig. 2a–c. Two additional characteristic example catchments are also highlighted for which hydrological modelling results are presented in Fig. 9. The three panels at the bottom illustrate the three GEV tail behaviours associated with the value of ξ, namely Weibull (ξ < 0), Gumbel (ξ ≈ 0), and Fréchet (ξ > 0).

https://doi.org/10.5194/egusphere-2026-4226
Preprint. Discussion started: 28 July 2026

conditions (Fig. 3a). The shape parameter controls the tail behaviour of the annual maximum storage deficits (S_d). We largely found negative ξ-values, indicative of bounded (Weibull-type) extremes, in water-limited regions such as western side of North America, southern Africa, northern India, Spain, eastern Brazil and Australia. In contrast, positive ξ-values, associated with heavy-tailed (Fréchet-type) behaviour, are more frequently observed in energy-limited and humid regions, particularly in eastern North America, northern Europe, southern Brazil, and New Zealand. Transitional hydroclimatic regions (Aridity Index $I_A = E_P/P = 0.5$–1) generally exhibit a mix of near-zero ξ-values that usually corresponds to approximately Gumbel-type behaviour. The overall distribution of ξ-values across all studied catchments is skewed towards slightly negative values with approximately 67% of the catchments exhibiting $\xi < 0$ (inset Fig. 3a) suggesting that the bounded extremes (Weibull-type) are globally more common than heavy-tailed extremes (Fréchet-type). This behaviour is further shown in the boxplot (inset Fig. 3a), where the shape parameter values decrease systematically with increasing aridity index with transitioning from slightly positive values in humid regions ($I_A < 1$) to predominantly negative values in more arid regions ($I_A > 1.5$). The same relationship is also evident in the Budyko framework plot (Fig. 3b), where catchments with heavier-tailed behaviour ($\xi > 0$) are mostly clustered in energy-limited regions and bounded extremes ($\xi < 0$) dominate water-limited regions.

The above plots (Fig. 3) indicate a distinct relationship between hydroclimatic conditions and the shape parameter. When analysed in the form of scatter plots (Fig. 4), it is found that the ξ exhibits a moderate but statistically significant correlation with aridity index I_A (Pearson $\rho = -0.48$, p-value < 0.001; Fig. 4a). A negative correlation indicates a tendency towards more negative ξ-values with increasing I_A. Similarly, ξ also shows a moderate, significant negative relation with evaporative index I_E ($\rho = -0.47$, p-value < 0.001; Fig. 4b) indicating that catchments with higher values of I_E are generally associated with bounded extremes. Overall, catchments located in more arid and water-limited regions tend to exhibit negative ξ values, whereas humid and energy-limited regions are generally associated with positive ξ values. Although, as can be seen from these figures, considerable scatter exists, the overall pattern is consistent with the behaviour observed in Fig. 3, suggesting a clear hydroclimatic control on the tail behaviour of annual maximum storage deficits across the studied catchments and its implications for uncertainty in $S_{r,max}$ estimates within the extended memory method framework.

https://doi.org/10.5194/egusphere-2026-4226
Preprint. Discussion started: 28 July 2026

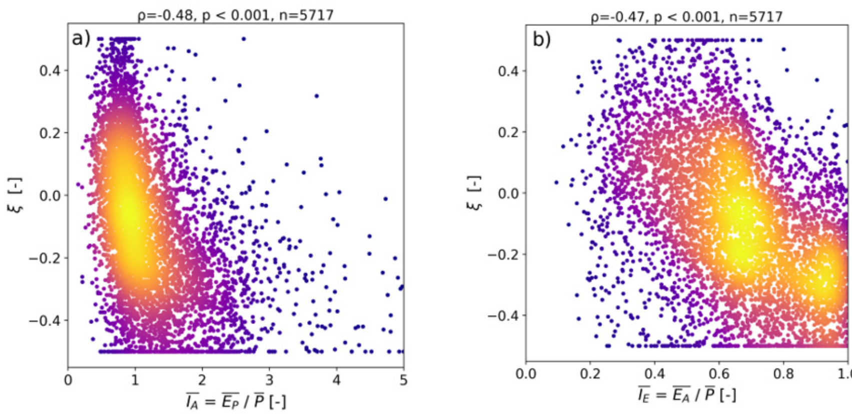

Figure 4: Spearman correlation coefficient (ρ) between the GEV shape parameter (ξ) and (a) aridity index (I_A) and (b) evaporative index (I_E). Each point here represents an individual catchment, while colour gradient indicates points density. The corresponding Spearman corelation coefficient (ρ), p-value, and number of catchments (n) are shown. For catchments with unrealistically high or low ξ estimates leading to unstable $S_{r,max}$ extrapolation at large return periods, ξ-values were constrained to ±0.5 to have realistic estimates of $S_{r,max}$.

The uncertainty in $S_{r,max}$ estimates, arising from the choice of the GEV distribution and return period selection, is quantified using bootstrap resampling and expressed as confidence bounds across return periods (5–80 years) (Fig. 5). It exhibits a pronounced dependence on hydroclimatic conditions. Across the studied catchments, uncertainty widths vary substantially with the largest ranges observed in transitional climates (I_A = 0.5–2) which show the widest uncertainty envelopes, with median ranges of approximately ± 66 mm. In contrast, both arid and humid regions exhibit comparatively narrower uncertainty widths, with median ranges of approximately ± 36 mm. This non-linear pattern indicates that uncertainty is not uniformly distributed across climatic regions but instead highest in regions where water and energy limitations are of comparable magnitudes. This pattern is also reflected in the three characteristic example catchments shown in Fig. 2. A catchment in arid region (I_A = 2.3; Fig. 2a), exhibiting Weibull-type behaviour has uncertainty width of ≈ 60 mm, whereas a catchment in humid region (I_A = 0.43; Fig. 2c), exhibiting Fréchet-type behaviour has an uncertainty width of ≈ 26. In contrast, a catchment in transitional climate (I_A = 0.73 ; Fig. 2b) which exhibits Gumbel-type behaviour has a substantially larger uncertainty width of ≈ 152 mm.

https://doi.org/10.5194/egusphere-2026-4226
Preprint. Discussion started: 28 July 2026

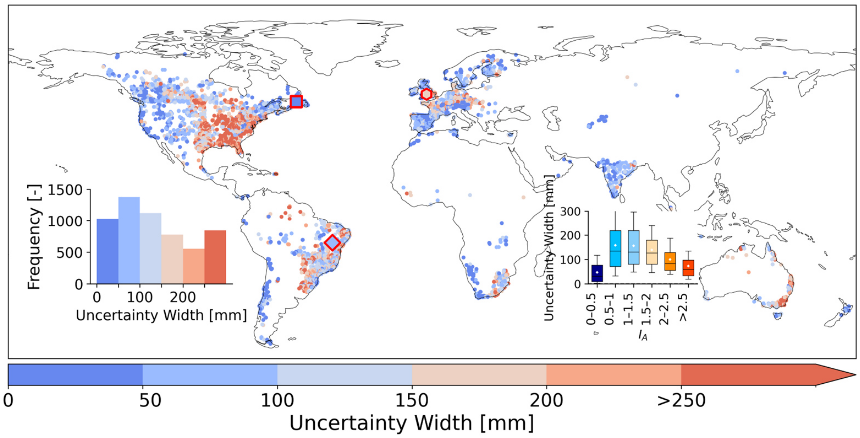

Figure 5: Global distribution of uncertainty width for the study catchments, calculated following the methodology illustrated in Fig. 2a. The highlighted catchments show the uncertainty widths of the three characteristic example catchments presented in Fig. 2a–c, which illustrates different GEV tail behaviours. The inset boxplots show the variation of uncertainty width across different aridity index classes. The boxplots illustrate 25th –75th percentile range, whiskers extend to the 10th and 90th percentiles, white diamonds denote the arithmetic means, and outliers are excluded for better visualization.

Even after accounting for uncertainty bounds associated with GEV-based estimates and return period selection into hydrological model calibration, a strong agreement is observed between memory method derived $S_{r,max}$ estimates and median calibrated $S_{r,max}$ values across the studied catchments (Fig. 6). At global scale (Fig. 6a; n = 2111), a strong and statistically significant relationship with $\rho = 0.93$ ($p < 0.001$) and a root mean square error (*RMSE*) of ~52 mm emerges. The median calibrated $S_{r,max}$ values closely follow the 1:1 line with memory method based estimates of $S_{r,max}$. This pattern indicates that the memory method based estimates of $S_{r,max}$ are, overall, robust and consistent with the values obtained through model calibration. The same strong agreement persists across different Köppen–Geiger hydroclimatic regions (Fig. 6b–f) with ρ remain high across all climate zones, ranging from 0.91–0.98 and *RMSE* values generally below 58 mm. In particular, catchments in Mediterranean (fig. 6d) and arid climates (Fig. 6f) exhibit very strong and almost unbiased relationships. While still strongly correlated, a higher fraction of catchments in cold (Fig. 6b) and temperate regions (Fig. 6c) are characterized by a somewhat stronger bias in the median calibrated estimates of $S_{r,max}$. This tendency is also reflected in the inset boxplots, which show broadly comparable distributions of calibrated and memory method based $S_{r,max}$ values across all climate regions.

https://doi.org/10.5194/egusphere-2026-4226
Preprint. Discussion started: 28 July 2026

However, the overall global consistency indicates that the relationship between memory method based and median calibrated $S_{r,max}$ is largely independent of climate.

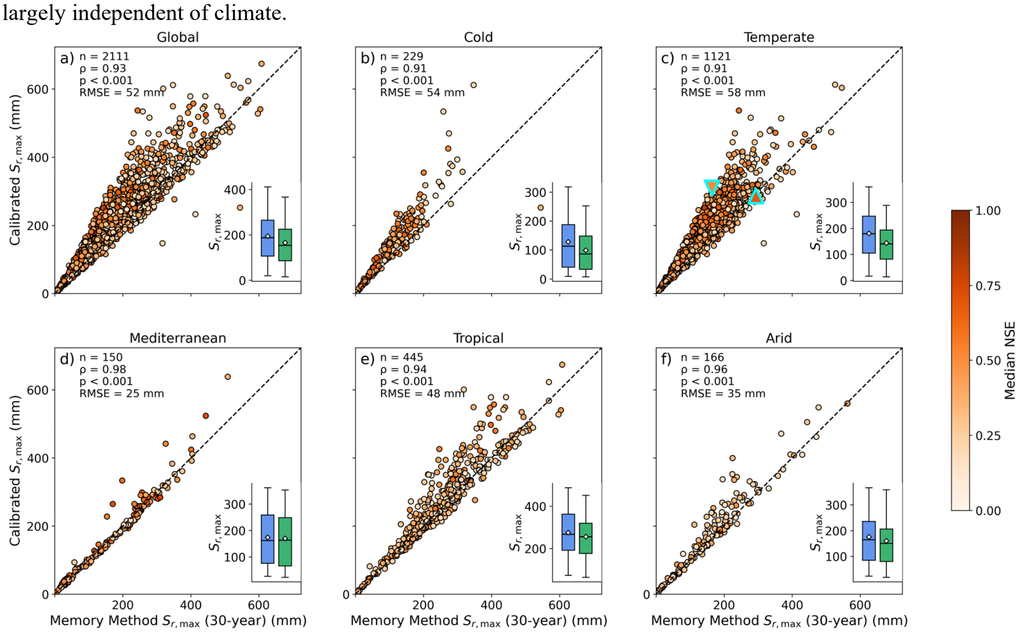

Figure 6: Spearman corelation coefficient (*ρ*) between memory method based $S_{r,max}$ (30-year return period) and median calibrated $S_{r,max}$ values (obtained as the median of the top 150 Pareto-optimal solutions). The colour gradient represents the median NSE_Q value between observed discharge and the median simulated discharge from the Pareto-optimal solutions. The inset boxplots compare the distributions of median calibrated $S_{r,max}$ values (left) and memory method based $S_{r,max}$ estimates (right) for each panel. The boxplots illustrate 25th –75th percentile range, whiskers extend to the 10th and 90th percentiles, white diamonds denote the arithmetic means, and outliers are excluded for better visualization. The number of catchments (n), Spearman corelation coefficient (*ρ*), p-value and *RMSE* are shown in each panel for a) Global scale and the five Köppen–Geiger climate regions defined in Fig. 1d: b) cold, c) temperate, d) Mediterranean, e) tropical, and f) arid. The highlighted points in panel c represent two characteristic example catchments for which the hydrological modelling results are presented in Fig. 9.

The relationship between the memory method and the median calibrated $S_{r,max}$ values nevertheless shows a clear sensitivity to the choice of return period within the memory method framework (Fig. 7). At the global scale, the Pearson correlation coefficient between the memory method and the median calibrated $S_{r,max}$ increases almost steadily with increase in return period, from relatively low values of ρ = 0.73–0.89 for return periods of 1.5–10 years to a maximum corelation of approximately ρ = 0.93 for a 30-year return period and after that the correlation gradually declines again. When stratified according to Köppen–Geiger climate zones, a similar pattern is observed in cold and temperate regions, where highest corelations (ρ = 0.91) are observed for return periods of 20–30 years, followed by a decline both for shorter and longer return periods. A sharp decline is more evident in temperate regions where it reduces to ρ = 0.61 for a return period of 80 years. In tropical and arid regions, correlations show a consistent increase up to around 20–30 years (ρ = 0.92–0.96), followed by a

https://doi.org/10.5194/egusphere-2026-4226
Preprint. Discussion started: 28 July 2026

relatively stable behaviour at higher return periods. In contrast, Mediterranean regions show consistently high correlations across all return periods, with values already exceeding 0.90 at short return periods and remains largely stable after 20–30 years. Overall, the results demonstrate a clear dependence of highest agreement between the memory method and median calibrated $S_{r,max}$ for a return period of 20–30 years across the different climate regions.

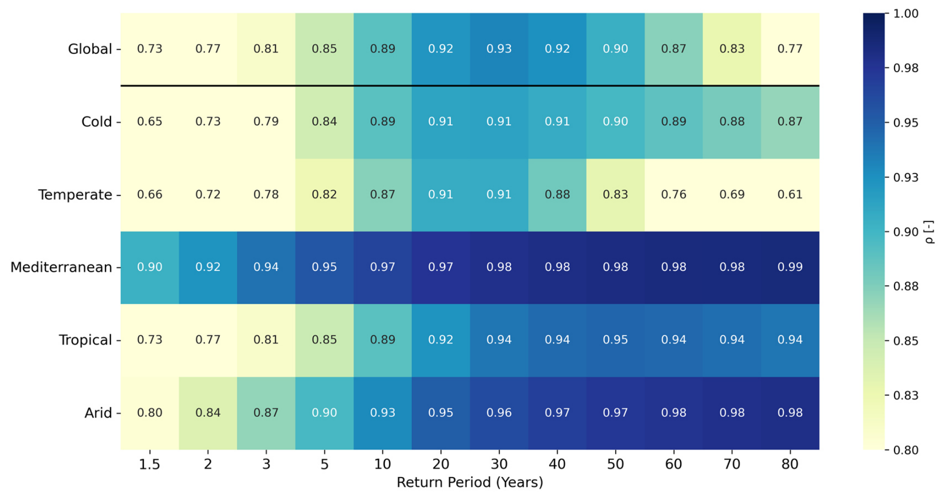

Figure 7: Sensitivity matrix of Spearman corelation coefficient (ρ) between memory method based $S_{r,max}$ estimates calculated for different return periods and median calibrated $S_{r,max}$ values obtained as the median of the top 150 Pareto-optimal solutions. Results are shown at Global scale and the five Köppen–Geiger climate regions defined in Fig. 1d: cold, temperate, Mediterranean, tropical, and arid.

The above sensitivity of the relationship between the memory method and median calibrated $S_{r,max}$ values to return period selection was further stratified according to the seasonality index (I_S) of liquid precipitation input, which revealed an additional hydroclimatic control (Fig. 8). For cold and temperate regions with relatively low seasonality ($I_S \leq 0.5$), the pattern as observed in Fig. 7 for cold and temperate regions persists where correlations are highest for return periods of 20–30 years and gradually decline for both shorter and longer return periods. In contrast, when $I_S > 0.5$, a different behaviour emerges across all climatic regions, where correlations increase gradually up to return periods of approximately 20–30 years and remain comparatively stable thereafter. These results indicate that the sensitivity of $S_{r,max}$ estimates to return period selection in cold

https://doi.org/10.5194/egusphere-2026-4226
Preprint. Discussion started: 28 July 2026

and temperate regions depends strongly on the I_S. However, for the remaining climatic regions, the sensitivity pattern remains comparatively stable after 20–30 years irrespective of whether I_S is above or below 0.5.

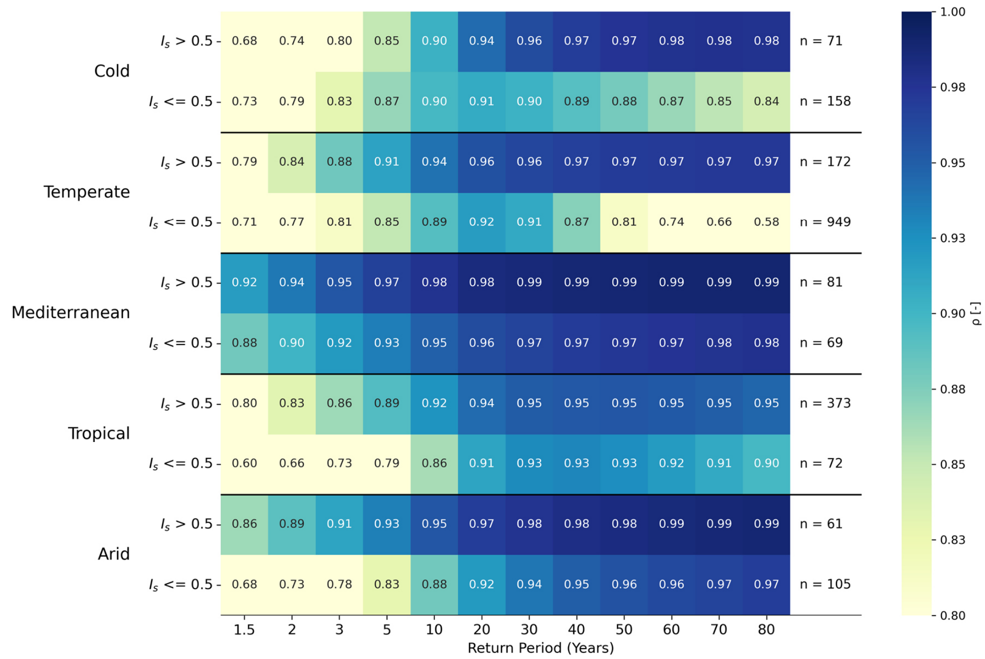

Figure 8: Sensitivity matrix of Spearman corelation coefficient (ρ) between memory method based $S_{r,max}$ estimates calculated for different return periods and median calibrated $S_{r,max}$ values obtained as the median of the top 150 Pareto-optimal solutions, stratified according to the seasonality index of liquid precipitation input (I_S > 0.5 and $I_S \leq 5$. Results are shown for the five Köppen–Geiger climate regions defined in Fig. 1d: cold, temperate, Mediterranean, tropical, and arid.

To further examine the relationship between memory method and calibrated $S_{r,max}$ estimates at the catchment scale and its implications for hydrological modelling, a characteristic catchment (Chile; I_A = 0.50) showing strong agreement between both estimates was selected (Fig. 9a–c). For this catchment, the memory method $S_{r,max} \approx 289$ mm is found to be very close to the median calibrated $S_{r,max} \approx 286$ mm (Fig. 9a). The distribution of calibrated $S_{r,max}$ values derived from the Pareto-optimal solutions (Fig. 9a, left) and memory method based $S_{r,max}$ values (Fig. 9a, right) shows a substantial overlap. The memory method based estimates are confined to a narrower range (≈ 270–300 mm) than the calibrated estimates (≈ 255–310 mm). Nevertheless, both distributions are centred around similar values of $S_{r,max}$. To evaluate the implications of these similar $S_{r,max}$ values on model performance, the observed daily discharge was compared with simulations generated using (i) the median simulated discharge obtained from all Pareto-optimal solutions and (ii) a model configuration in which the memory

https://doi.org/10.5194/egusphere-2026-4226
Preprint. Discussion started: 28 July 2026

method $S_{r,max}$ was fixed during calibration. Both approaches resulted in modelled hydrographs that closely match with the observed discharge with NSE_Q values ranging between 0.72–0.74 and $NSE_{log(Q)}$ values between 0.73–0.81. In both cases, the timing and magnitudes of major flow events were well captured. It is pertinent to mention that these performance indicator values were calculated by comparing observed discharge with the median simulated discharge from each modelling approach. Furthermore, the distributions of performance indicators across all Pareto-optimal solutions for both modelling approaches exhibit similar distributions with NSE_Q values ranging from 0.59 to 0.74 and $NSE_{log(Q)}$ values ranging from 0.68 to 0.84 respectively (Fig. 9c).

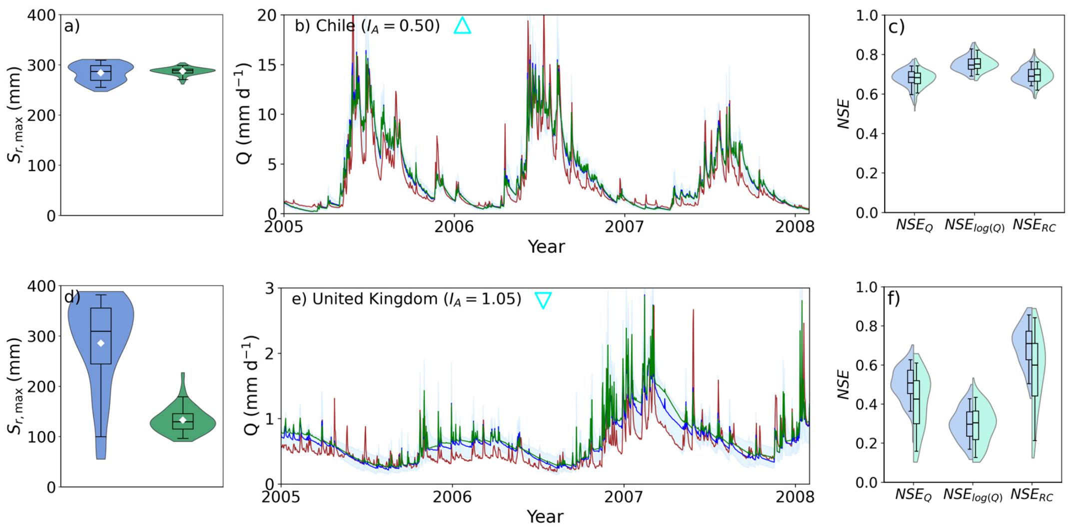

Figure 9: Characteristic example catchments in temperate region where panels a–c shows a strong agreement and panels d–f shows a weaker agreement between memory method based and calibrated $S_{r,max}$ estimates. These catchments are the highlighted catchments shown in Figs. 3 and 6. Panels b and e: Comparison of observed discharge (Q; brown line) with median simulated discharge (dark blue line) obtained from Pareto-optimal solutions. The light blue shaded area shows the 5th and 95th percentiles range of simulated discharge from the Pareto-optimal solutions. The green line shows the median simulated discharge obtained using a fixed value of $S_{r,max}$ derived from the memory method for a return period of 20-year. Panels a) and d): The left distribution shows calibrated $S_{r,max}$ values from the Pareto-optimal solutions, while the right distribution shows memory method based $S_{r,max}$ estimates for a 20-year return period derived from each bootstrap sample (light colour lines Fig. 2). Panels c) and f): Model performance indicators (NSE_Q, $NSE_{log(Q)}$, and NSE_{RC}) for all Pareto-optimal solutions. The left half shows the distribution of performance indicators obtained from standard calibration, in which $S_{r,max}$ was calibrated over a range (Fig. 2a). The right half shows the distributions of performance indicators for the model configuration in which $S_{r,max}$ value was fixed as obtained from memory method for a return period of 20-year.

In contrast to the previous example, another characteristic catchment (United Kingdom; I_A = 1.05) exhibits a weaker agreement between the memory method and calibrated $S_{r,max}$ estimates (Fig. 9d–e). For this catchment, the memory method $S_{r,max} \approx 130$ mm is substantially lower than the median calibrated $S_{r,max} \approx 310$ mm (Fig. 9d) obtained from the retained Pareto-optimal solutions. The distributions of calibrated $S_{r,max}$ values and memory method $S_{r,max}$ estimates show only a minor overlap, with the memory method generally underestimating $S_{r,max}$ (Fig. 9d). Although both approaches generally capture the overall discharge dynamics during the analysis period, noticeable differences are observed for several peak flow events (Fig. 9e). The median simulated discharge obtained from the retained calibrated solutions results in NSE_Q and $NSE_{log(Q)}$ values of 0.68 and 0.50, respectively, while the model configuration with fixed memory method $S_{r,max}$ yields values of 0.49 and 0.36, respectively. Overall, model performance was found to be slightly lower than for the previous example catchment (Fig. 9a–c). Nevertheless, the distributions of the performance indicators for the Pareto-optimal solutions remain broadly similar for the two modelling approaches (Fig. 9f). For example, the distributions of NSE_Q and $NSE_{log(Q)}$ largely overlap with values ≈ 0.17–0.62 and ≈ 0.12–0.42 respectively. These results indicate that despite of having large differences in the $S_{r,max}$ values, constraining the model with the memory method $S_{r,max}$ estimate yields model performance that is broadly comparable to that achieved from standard calibration approach.

4 Discussion

Uncertainty in root zone storage capacity $S_{r,max}$ has important implications for hydrological modelling as it controls the partitioning of water fluxes (Milly, 2001; Donohue et al., 2007; Ibrahim et al., 2026). In this study we extended the widely used memory method by replacing the commonly used fixed Gumbel assumption with a GEV distribution, allowing for a more flexible representation of extreme annual storage deficits. Applying this extended framework at global scale (~5700 catchments), we have found that GEV shape parameter ξ shows a clear dependence on hydroclimatic conditions. Negative ξ-values, associated with bounded extremes are predominantly found in water-limited regions whereas positive values indicative of heavy tailed behaviour are found in humid and energy-limited regions. This behaviour is consistent with the notion that hydrological extremes are constrained by different limiting processes in dry and humid environments. In dry and water-limited catchments, strong evaporative demand and limited water availability tend to constrain the magnitude of storage deficits leading to more bounded extremes behaviour (Donat et al., 2019). Even if vegetation extended its root systems, insufficient water is stored in the subsurface to sustain high levels of transpiration. To limit inefficient and ineffective subsurface resource investment in the absence of sufficient subsurface water, vegetation therefore does not further extend its root systems and consequently $S_{r,max}$ converges towards bounded extremes, i.e. negative ξ-values thus in water-limited environments. In contrast, for humid and energy-limited regions, abundant water availability with variable atmospheric forcing, results in greater variability and heavy tailed behaviour in hydrological extremes. In other words, the positive ξ-values in such humid climates, and in stark contrast to the above arid climates, are a manifestation that vegetation can considerably benefit from extending its

https://doi.org/10.5194/egusphere-2026-4226
Preprint. Discussion started: 28 July 2026

root zones (and thus $S_{r,max}$) as sufficient water is available in the subsurface and can be accessed for use in dry periods if root systems are extensive enough.

The hydroclimatic dependence of ξ is further also reflected in the uncertainty widths associated with $S_{r,max}$ estimates (inset Fig. 5). The largest uncertainty widths are observed in transitional climates (I_A = 0.5–2) where water and energy limitations are of equal importance. In these intermediate regions, annual maximum storage deficits are generally moderate under normal conditions but can occasionally become very large during more severe dry periods. As a result, the difference between frequently occurring deficits and rare extreme deficits becomes much larger, leading to wider uncertainty ranges in $S_{r,max}$ estimates. Arid and humid regions are characterized by comparatively narrow uncertainty widths as observed in characteristic example catchments shown in Fig. 2a and 2c. As mentioned earlier, for arid regions, storage deficits are already consistently high and physically constrained by limited water availability, resulting in relatively smaller increases in $S_{r,max}$ with increasing return period that ultimately yields to narrow uncertainty width in $S_{r,max}$ estimates. The narrower uncertainty widths observed in humid regions despite of mostly heavy tailed behaviour for majority of the catchments can likely be attributed to frequent rainfall events and sustained moisture availability which tend to interrupt and limit the prolonged accumulation of storage deficits. As a result, they are less extreme in magnitude than those in transitional climates leading to narrower uncertainty widths of $S_{r,max}$. This behaviour is consistent with extreme value theory, where return level estimates are sensitive to model assumptions and extrapolation uncertainty (Katz et al., 2002).

The strong agreement between memory method based and calibrated $S_{r,max}$ estimates both at global scale and across different Koppen Geiger climatic zones (Fig. 6) supports the robustness of the memory method despite the uncertainty associated with extreme value representation and return period selection. Previous studies using the original memory method framework based on a fixed Gumbel distribution have similarly shown that memory method derived $S_{r,max}$ estimates can adequately reproduce model calibrated $S_{r,max}$ estimates at local and regional scales (Gao et al., 2014; Bouaziz et al., 2022; Wang et al., 2024). Our analysis extends these findings to a substantially larger global dataset spanning diverse hydroclimatic conditions while additionally accounting for uncertainty through the use of a more flexible GEV framework. Nevertheless, systematic differences between memory method and calibrated $S_{r,max}$ estimates are observed in some climatic regions. For example, memory method based $S_{r,max}$ tends to underestimate $S_{r,max}$ in cold and temperate region catchments (Fig. 6b–c) relative to median calibrated $S_{r,max}$ values. The reason for this underestimation remains unclear and require further research. In contrast, comparatively stronger agreement is observed in Mediterranean, tropical, and arid regions, where memory method estimates closely align with median calibrated $S_{r,max}$ values across a wide range of hydroclimatic conditions.

In this study, we have found a clear sensitivity of memory method $S_{r,max}$ estimates to return period selection across different climatic regions. Although the agreement between memory method and median calibrated $S_{r,max}$ values generally

https://doi.org/10.5194/egusphere-2026-4226
Preprint. Discussion started: 28 July 2026

improves with an increase in return period, the strongest corelations are consistently observed around return periods of approximately 20–30 years (Fig. 7). Beyond this range, correlations either gradually decline or stabilize depending on the hydroclimatic conditions. The emergence of this optimal return period across contrasting climatic regions is particularly notable given the differences in tail behaviour that we have found through GEV analysis. Previous studies (Gao et al., 2014; De Boer-Euser et al., 2016; Nijzink et al., 2016; Wang-Erlandsson et al., 2016; Bouaziz et al., 2020; Tempel et al., 2024) commonly adopted a fixed 20-year return period largely based on empirical and ecohydrological reasoning related to vegetation adaptation to drought conditions. Our results provide an additional large sample support for this assumption while also showing that the sensitivity to return period selection varies with hydroclimatic seasonality (Fig. 8). In particular catchments in cold and temperate regions with low seasonality exhibit highest corelations around 20–30 years and declines afterwards, whereas catchments with high seasonality generally show more stable correlations beyond of this range. This behaviour suggests that the influence of extreme storage deficits on $S_{r,max}$ estimation may differ between more seasonal persistent and more event driven catchments.

The global scale analysis demonstrates a strong agreement between memory method based and median calibrated $S_{r,max}$ estimate despite the uncertainties associated with distributional assumptions and return period selection. The catchment scale analysis further illustrates both the strengths and limitations of the memory method at individual catchment scale. For the first example catchment (Fig. 9a–c), the memory method and median calibrated $S_{r,max}$ estimates closely match with each other, and both model configurations produced highly similar hydrographs. In contrast, for the second example catchment (Fig. 9d–f), though differences between the memory method and median calibrated $S_{r,max}$ estimates exist, the discharge dynamics were reasonably well captured by both. These contrasting examples, highlights that comparable streamflow performance can be achieved across a relatively wide range of $S_{r,max}$ values. This behaviour reflects a classic example of equifinality in hydrological modelling, where different parameter combinations can produce comparable model performance by compensating each other (Beven and Freer, 2001). Even in cases where the calibrated $S_{r,max}$ distributions span relatively a wide range (Fig. 9d), many of these parameter sets can produce almost equally good performance in terms of performance indicators indicating that similar streamflow simulations can be achieved despite differences in estimated $S_{r,max}$ values.

Overall, a strong agreement between memory method and median calibrated $S_{r,max}$ estimates suggests that the memory method provides a physically meaningful estimate of vegetation accessible storage at the catchment scale. By constraining $S_{r,max}$ derived from memory method, we can reduce the calibration burden and number of calibration parameters, and thus most importantly the associated uncertainty in large scale hydrological and land-surface models. These findings are consistent with other studies showing that climate-based estimates of $S_{r,max}$ are closely linked to long-term vegetation adaptation strategies under drought conditions (Gao et al., 2014; Wang-Erlandsson et al., 2016; Van Oorschot et al., 2021). However, the present

https://doi.org/10.5194/egusphere-2026-4226
Preprint. Discussion started: 28 July 2026

study extends these findings by explicitly quantifying the uncertainty associated with distributional assumptions and return period selection within the memory method framework.

5 Conclusions

In this study, we systematically evaluated the uncertainties associated with memory method derived root zone storage capacity ($S_{r,max}$) estimates arising from 1) the use of a more flexible GEV distribution instead of a fixed Gumbel distribution and from 2) the selection of return periods across the global scale. We used ~5700 catchments for GEV analysis and ~2100 catchments for model calibration. The results show that the GEV shape parameter exhibits a clear hydroclimatic dependence with bounded extremes dominating water-limited regions and heavy tailed extremes occurring more frequently in humid and energy-limited region catchments. The $S_{r,max}$ uncertainty width is not uniform but systematically varies across climates, with the widest ranges observed in transitional regions (± 66 mm) compared to arid and humid regions (± 36 mm). The memory method based estimates of $S_{r,max}$ show strong agreement with median calibrated $S_{r,max}$ values ($\rho = 0.93$). The highest corelation ($\rho = 0.91$–0.98) is consistently found for return periods of 20–30 years across climatic region, providing a large sample support for the commonly used 20-year return period assumption. Overall, the findings of this study demonstrates that the memory method based estimates of $S_{r,max}$ can serve as a reliable constraint in hydrological model calibration, reducing parameter uncertainty and equifinality without compromising hydrological model performance.

Data availability. All datasets used in this study are publicly accessible and can be obtained from the sources listed in Table 1.

Author contributions. This study was conceptualized by MI, MH, MCG, and RvdE. MI carried out the formal analysis and drafted the manuscript with contributions and revisions from MH, MCG, and RvdE

Competing interests. MCG and MH are members of the Editorial Board of HESS. The authors have no other competing interests to declare.

Financial support. This work was funded by Higher Education Commission of Pakistan (grant no. Ref:1(2)/HRD/OSSIII/2021/HEC/19607).

References

Alvarez-Garreton, C., Mendoza, P. A., Boisier, J. P., Addor, N., Galleguillos, M., Zambrano-Bigiarini, M., Lara, A., Puelma, C., Cortes, G., Garreaud, R., McPhee, J., and Ayala, A.: The CAMELS-CL dataset: catchment attributes and meteorology for large sample studies – Chile dataset, Hydrology and Earth System Sciences, 22, 5817-5846,https://doi.org/10.5194/hess-22-5817-2018, 2018.

Arsenault, R., Brissette, F., Martel, J. L., Troin, M., Levesque, G., Davidson-Chaput, J., Gonzalez, M. C., Ameli, A., and Poulin, A.: A comprehensive, multisource database for hydrometeorological modeling of 14,425 North American watersheds, Sci Data, 7, 243,https://doi.org/10.1038/s41597-020-00583-2, 2020.

Beven, K.: Validation and equifinality, in: Computer simulation validation: Fundamental concepts, methodological frameworks, and philosophical perspectives, Springer, 791-809,https://doi.org/10.1007/978-3-319-70766-2_32, 2019.

Beven, K. and Freer, J.: Equifinality, data assimilation, and uncertainty estimation in mechanistic modelling of complex environmental systems using the GLUE methodology, Journal of hydrology, 249, 11-29,https://doi.org/10.1016/S0022-1694(01)00421-8, 2001.

Boardman, E. N., Boisramé, G. F. S., Wigmosta, M. S., Shriver, R. K., and Harpold, A. A.: Improving model calibrations in a changing world: controlling for nonstationarity after mega disturbance reduces hydrological uncertainty, Hydrology and Earth System Sciences, 29, 6333-6352,https://doi.org/10.5194/hess-29-6333-2025, 2025.

Bouaziz, L. J. E., Steele-Dunne, S. C., Schellekens, J., Weerts, A. H., Stam, J., Sprokkereef, E., Winsemius, H. H. C., Savenije, H. H. G., and Hrachowitz, M.: Improved Understanding of the Link Between Catchment-Scale Vegetation Accessible Storage and Satellite-Derived Soil Water Index, Water Resources Research, 56,https://doi.org/10.1029/2019wr026365, 2020.

Bouaziz, L. J. E., Aalbers, E. E., Weerts, A. H., Hegnauer, M., Buiteveld, H., Lammersen, R., Stam, J., Sprokkereef, E., Savenije, H. H. G., and Hrachowitz, M.: Ecosystem adaptation to climate change: the sensitivity of hydrological predictions to time-dynamic model parameters, Hydrology and Earth System Sciences, 26, 1295-1318,https://doi.org/10.5194/hess-26-1295-2022, 2022.

Bushra, S., Shakya, J., Cattoën, C., Fischer, S., and Pahlow, M.: CAMELS-NZ: hydrometeorological time series and landscape attributes for New Zealand, Earth System Science Data, 17, 5745-5760,https://doi.org/10.5194/essd-17-5745-2025, 2025.

Chagas, V. B. P., Chaffe, P. L. B., Addor, N., Fan, F. M., Fleischmann, A. S., Paiva, R. C. D., and Siqueira, V. A.: CAMELS-BR: hydrometeorological time series and landscape attributes for 897 catchments in Brazil, Earth System Science Data, 12, 2075-2096,https://doi.org/10.5194/essd-12-2075-2020, 2020.

Clark, M. P., Fan, Y., Lawrence, D. M., Adam, J. C., Bolster, D., Gochis, D. J., Hooper, R. P., Kumar, M., Leung, L. R., Mackay, D. S., Maxwell, R. M., Shen, C., Swenson, S. C., and Zeng, X.: Improving the representation of hydrologic processes in Earth System Models, Water Resources Research, 51, 5929-5956,https://doi.org/10.1002/2015wr017096, 2015.

Coenders-Gerrits, A. M., van der Ent, R. J., Bogaard, T. A., Wang-Erlandsson, L., Hrachowitz, M., and Savenije, H. H.: Uncertainties in transpiration estimates, Nature, 506, E1-2,https://doi.org/10.1038/nature12925, 2014.

Coles, S., Bawa, J., Trenner, L., and Dorazio, P.: An introduction to statistical modeling of extreme values, Springer,https://doi.org/10.1007/978-1-4471-3675-0, 2001.

Coxon, G., Addor, N., Bloomfield, J. P., Freer, J., Fry, M., Hannaford, J., Howden, N. J. K., Lane, R., Lewis, M., Robinson, E. L., Wagener, T., and Woods, R.: CAMELS-GB: hydrometeorological time series and landscape attributes for 671 catchments in Great Britain, Earth System Science Data, 12, 2459-2483,https://doi.org/10.5194/essd-12-2459-2020, 2020.

de Boer-Euser, T., McMillan, H. K., Hrachowitz, M., Winsemius, H. C., and Savenije, H. H. G.: Influence of soil and climate on root zone storage capacity, Water Resources Research, 52, 2009-2024,https://doi.org/10.1002/2015wr018115, 2016.

Delaigue, O., Guimarães, G. M., Brigode, P., Génot, B., Perrin, C., Soubeyroux, J.-M., Janet, B., Addor, N., and Andréassian, V.: CAMELS-FR dataset: a large-sample hydroclimatic dataset for France to explore hydrological diversity and support model benchmarking, Earth System Science Data, 17, 1461-1479,https://doi.org/10.5194/essd-17-1461-2025, 2025.

Dirmeyer, P. A., Gao, X., Zhao, M., Guo, Z., Oki, T., and Hanasaki, N.: GSWP-2: Multimodel analysis and implications for our perception of the land surface, Bulletin of the American Meteorological Society, 87, 1381-1398,https://doi.org/10.1175/BAMS-87-10-1381, 2006.

Do, H. X., Gudmundsson, L., Leonard, M., and Westra, S.: The Global Streamflow Indices and Metadata Archive (GSIM) – Part 1: The production of a daily streamflow archive and metadata, Earth System Science Data, 10, 765-785,https://doi.org/10.5194/essd-10-765-2018, 2018.

do Nascimento, T. V. M., Rudlang, J., Hoge, M., van der Ent, R., Chappon, M., Seibert, J., Hrachowitz, M., and Fenicia, F.: EStreams: An integrated dataset and catalogue of streamflow, hydro-climatic and landscape variables for Europe, Sci Data, 11, 879,https://doi.org/10.1038/s41597-024-03706-1, 2024.

Donat, M. G., Angélil, O., and Ukkola, A. M.: Intensification of precipitation extremes in the world’s humid and water-limited regions, Environmental Research Letters, 14,https://doi.org/10.1088/1748-9326/ab1c8e, 2019.

Donohue, R., Roderick, M., and McVicar, T. R.: On the importance of including vegetation dynamics in Budyko's hydrological model, Hydrology and Earth System Sciences, 11, 983-995,https://doi.org/10.5194/hess-11-983-2007, 2007.

Donohue, R. J., Roderick, M. L., and McVicar, T. R.: Roots, storms and soil pores: Incorporating key ecohydrological processes into Budyko’s hydrological model, Journal of Hydrology, 436-437, 35-50,https://doi.org/10.1016/j.jhydrol.2012.02.033, 2012.

Dralle, D. N., Hahm, W. J., Chadwick, K. D., McCormick, E., and Rempe, D. M.: Technical note: Accounting for snow in the estimation of root zone water storage capacity from precipitation and evapotranspiration fluxes, Hydrology and Earth System Sciences, 25, 2861-2867,https://doi.org/10.5194/hess-25-2861-2021, 2021.

Fatichi, S., Pappas, C., and Ivanov, V. Y.: Modeling plant–water interactions: an ecohydrological overview from the cell to the global scale, WIREs Water, 3, 327-368,https://doi.org/10.1002/wat2.1125, 2015.

Fowler, K. J. A., Acharya, S. C., Addor, N., Chou, C., and Peel, M. C.: CAMELS-AUS: hydrometeorological time series and landscape attributes for 222 catchments in Australia, Earth System Science Data, 13, 3847-3867,https://doi.org/10.5194/essd-13-3847-2021, 2021.

Gao, H., Hrachowitz, M., Schymanski, S. J., Fenicia, F., Sriwongsitanon, N., and Savenije, H. H. G.: Climate controls how ecosystems size the root zone storage capacity at catchment scale, Geophysical Research Letters, 41, 7916-7923,https://doi.org/10.1002/2014gl061668, 2014.

Gao, H., Hrachowitz, M., Wang-Erlandsson, L., Fenicia, F., Xi, Q., Xia, J., Shao, W., Sun, G., and Savenije, H. H. G.: Root zone in the Earth system, Hydrology and Earth System Sciences, 28, 4477-4499,https://doi.org/10.5194/hess-28-4477-2024, 2024.

Gentine, P., D'Odorico, P., Lintner, B. R., Sivandran, G., and Salvucci, G.: Interdependence of climate, soil, and vegetation as constrained by the Budyko curve, Geophysical Research Letters, 39, L19404,https://doi.org/10.1029/2012gl053492, 2012.

Gudmundsson, L., Do, H. X., Leonard, M., and Westra, S.: The Global Streamflow Indices and Metadata Archive (GSIM) – Part 2: Quality control, time-series indices and homogeneity assessment, Earth System Science Data, 10, 787-804,https://doi.org/10.5194/essd-10-787-2018, 2018.

Han, J., Yang, Y., Roderick, M. L., McVicar, T. R., Yang, D., Zhang, S., and Beck, H. E.: Assessing the Steady-State Assumption in Water Balance Calculation Across Global Catchments, Water Resources Research, 56, e2020WR027392,https://doi.org/10.1029/2020wr027392, 2020.

Hargreaves, G. H. and Samani, Z. A.: Estimating potential evapotranspiration, Journal of the irrigation and Drainage Division, 108, 225-230, 1982.

Hrachowitz, M. and Clark, M. P.: HESS Opinions: The complementary merits of competing modelling philosophies in hydrology, Hydrology and Earth System Sciences, 21, 3953-3973,https://doi.org/10.5194/hess-21-3953-2017, 2017.

Hrachowitz, M., Stockinger, M., Coenders-Gerrits, M., van der Ent, R., Bogena, H., Lücke, A., and Stumpp, C.: Reduction of vegetation-accessible water storage capacity after deforestation affects catchment travel time distributions and

increases young water fractions in a headwater catchment, Hydrology and Earth System Sciences, 25, 4887-4915,https://doi.org/10.5194/hess-25-4887-2021, 2021.
Hrachowitz, M., Fovet, O., Ruiz, L., Euser, T., Gharari, S., Nijzink, R., Freer, J., Savenije, H. H. G., and Gascuel-Odoux, C.: Process consistency in models: The importance of system signatures, expert knowledge, and process complexity, Water Resources Research, 50, 7445-7469,https://doi.org/10.1002/2014wr015484, 2014.
Hulsman, P., Winsemius, H. C., Michailovsky, C. I., Savenije, H. H. G., and Hrachowitz, M.: Using altimetry observations combined with GRACE to select parameter sets of a hydrological model in a data-scarce region, Hydrology and Earth System Sciences, 24, 3331-3359,https://doi.org/10.5194/hess-24-3331-2020, 2020.
Ibrahim, M., van Oorschot, F., van der Ent, R., Hrachowitz, M., and Coenders-Gerrits, M.: Catchment precipitation partitioning in the Budyko framework is controlled by root zone storage capacity, Environmental Research Letters, 21,https://doi.org/10.1088/1748-9326/ae612a, 2026.
Jasechko, S.: Plants turn on the tap, Nature Climate Change, 8, 562-563,https://doi.org/10.1038/s41558-018-0212-z, 2018.
Katz, R. W., Parlange, M. B., and Naveau, P.: Statistics of extremes in hydrology, Advances in water resources, 25, 1287-1304,https://doi.org/10.1016/S0309-1708(02)00056-8, 2002.
Kratzert, F., Nearing, G., Addor, N., Erickson, T., Gauch, M., Gilon, O., Gudmundsson, L., Hassidim, A., Klotz, D., Nevo, S., Shalev, G., and Matias, Y.: Caravan - A global community dataset for large-sample hydrology, Sci Data, 10, 61,https://doi.org/10.1038/s41597-023-01975-w, 2023.
Loritz, R., Dolich, A., Acuña Espinoza, E., Ebeling, P., Guse, B., Götte, J., Hassler, S. K., Hauffe, C., Heidbüchel, I., Kiesel, J., Mälicke, M., Müller-Thomy, H., Stölzle, M., and Tarasova, L.: CAMELS-DE: hydro-meteorological time series and attributes for 1582 catchments in Germany, Earth System Science Data, 16, 5625-5642,https://doi.org/10.5194/essd-16-5625-2024, 2024.
Mangukiya, N. K., Kumar, K. B., Dey, P., Sharma, S., Bejagam, V., Mujumdar, P. P., and Sharma, A.: CAMELS-IND: hydrometeorological time series and catchment attributes for 228 catchments in Peninsular India, Earth System Science Data, 17, 461-491,https://doi.org/10.5194/essd-17-461-2025, 2025.
Marti, B., Yakovlev, A., Karger, D. N., Ragettli, S., Zhumabaev, A., Wakil, A. W., and Siegfried, T.: CA-discharge: Geo-Located Discharge Time Series for Mountainous Rivers in Central Asia, Sci Data, 10, 579,https://doi.org/10.1038/s41597-023-02474-8, 2023.
McCormick, E. L., Dralle, D. N., Hahm, W. J., Tune, A. K., Schmidt, L. M., Chadwick, K. D., and Rempe, D. M.: Widespread woody plant use of water stored in bedrock, Nature, 597, 225-229,https://doi.org/10.1038/s41586-021-03761-3, 2021.
Milly, P.: Climate, soil water storage, and the average annual water balance, Water Resources Research, 30, 2143-2156,https://doi.org/10.1029/94WR00586, 1994.
Milly, P. C. D.: A minimalist probabilistic description of root zone soil water, Water Resources Research, 37, 457-463,https://doi.org/10.1029/2000wr900337, 2001.
Newman, A. J., Clark, M. P., Sampson, K., Wood, A., Hay, L. E., Bock, A., Viger, R. J., Blodgett, D., Brekke, L., Arnold, J. R., Hopson, T., and Duan, Q.: Development of a large-sample watershed-scale hydrometeorological data set for the contiguous USA: data set characteristics and assessment of regional variability in hydrologic model performance, Hydrology and Earth System Sciences, 19, 209-223,https://doi.org/10.5194/hess-19-209-2015, 2015.
Nijzink, R., Hutton, C., Pechlivanidis, I., Capell, R., Arheimer, B., Freer, J., Han, D., Wagener, T., McGuire, K., Savenije, H., and Hrachowitz, M.: The evolution of root-zone moisture capacities after deforestation: a step towards hydrological predictions under change?, Hydrology and Earth System Sciences, 20, 4775-4799,https://doi.org/10.5194/hess-20-4775-2016, 2016.
Ponds, M., Hanus, S., Zekollari, H., ten Veldhuis, M.-C., Schoups, G., Kaitna, R., and Hrachowitz, M.: Adaptation of root zone storage capacity to climate change and its effects on future streamflow in Alpine catchments: towards non-stationary model parameters, Hydrology and Earth System Sciences, 29, 3545-3568,https://doi.org/10.5194/hess-29-3545-2025, 2025.
Porporato, A., Daly, E., and Rodriguez-Iturbe, I.: Soil water balance and ecosystem response to climate change, The American Naturalist, 164, 625-632,https://doi.org/10.1086/424970, 2004.
Savenije, H. H. G. and Hrachowitz, M.: HESS Opinions Catchments as meta-organisms – a new blueprint for hydrological modelling, Hydrology and Earth System Sciences, 21, 1107-1116,https://doi.org/10.5194/hess-21-1107-2017, 2017.

https://doi.org/10.5194/egusphere-2026-4226
Preprint. Discussion started: 28 July 2026

Seneviratne, S. I., Corti, T., Davin, E. L., Hirschi, M., Jaeger, E. B., Lehner, I., Orlowsky, B., and Teuling, A. J.: Investigating soil moisture–climate interactions in a changing climate: A review, Earth-Science Reviews, 99, 125-161,https://doi.org/10.1016/j.earscirev.2010.02.004, 2010.

Stocker, B. D., Tumber-Davila, S. J., Konings, A. G., Anderson, M. C., Hain, C., and Jackson, R. B.: Global patterns of water storage in the rooting zones of vegetation, Nat Geosci, 16, 250-256,https://doi.org/10.1038/s41561-023-01125-2, 2023.

Tempel, N. T., Bouaziz, L., Taormina, R., van Noppen, E., Stam, J., Sprokkereef, E., and Hrachowitz, M.: Catchment response to climatic variability: implications for root zone storage and streamflow predictions, Hydrology and Earth System Sciences, 28, 4577-4597,https://doi.org/10.5194/hess-28-4577-2024, 2024.

Tramblay, Y., Rouché, N., Paturel, J.-E., Mahé, G., Boyer, J.-F., Amoussou, E., Bodian, A., Dacosta, H., Dakhlaoui, H., Dezetter, A., Hughes, D., Hanich, L., Peugeot, C., Tshimanga, R., and Lachassagne, P.: ADHI: the African Database of Hydrometric Indices (1950–2018), Earth System Science Data, 13, 1547-1560,https://doi.org/10.5194/essd-13-1547-2021, 2021.

van Oorschot, F., van der Ent, R. J., Alessandri, A., and Hrachowitz, M.: Influence of irrigation on root zone storage capacity estimation, Hydrology and Earth System Sciences, 28, 2313-2328,https://doi.org/10.5194/hess-28-2313-2024, 2024.

van Oorschot, F., van der Ent, R. J., Hrachowitz, M., and Alessandri, A.: Climate-controlled root zone parameters show potential to improve water flux simulations by land surface models, Earth System Dynamics, 12, 725-743,https://doi.org/10.5194/esd-12-725-2021, 2021.

Wang-Erlandsson, L., Bastiaanssen, W. G. M., Gao, H., Jägermeyr, J., Senay, G. B., van Dijk, A. I. J. M., Guerschman, J. P., Keys, P. W., Gordon, L. J., and Savenije, H. H. G.: Global root zone storage capacity from satellite-based evaporation, Hydrology and Earth System Sciences, 20, 1459-1481,https://doi.org/10.5194/hess-20-1459-2016, 2016.

Wang, S., Hrachowitz, M., and Schoups, G.: Multi-decadal fluctuations in root zone storage capacity through vegetation adaptation to hydro-climatic variability have minor effects on the hydrological response in the Neckar River basin, Germany, Hydrology and Earth System Sciences, 28, 4011-4033,https://doi.org/10.5194/hess-28-4011-2024, 2024.

Ye, S., Yaeger, M., Coopersmith, E., Cheng, L., and Sivapalan, M.: Exploring the physical controls of regional patterns of flow duration curves – Part 2: Role of seasonality, the regime curve, and associated process controls, Hydrology and Earth System Sciences, 16, 4447-4465,https://doi.org/10.5194/hess-16-4447-2012, 2012.

`